A model-based approach for the estimation of bearing forces and moments using outer-ring deformation

Kerst, Stijn; Shyrokau, Barys; Holweg, Edward

DOI
10.1109/TIE.2019.2897510

Publication date
2019

Document Version
Final published version

Published in
IEEE Transactions on Industrial Electronics

Citation (APA)
Kerst, S., Shyrokau, B., & Holweg, E. (2019). A model-based approach for the estimation of bearing forces and moments using outer-ring deformation. *IEEE Transactions on Industrial Electronics*, *67*(1), 461-470. https://doi.org/10.1109/TIE.2019.2897510

A Model-Based Approach for the Estimation of Bearing Forces and Moments Using Outer Ring Deformation

Stijn Kerst, Barys Shyrokau, and Edward Holweg

***Abstract*—Bearing load estimation would form a valuable addition to the fields of condition monitoring and system control. Despite effort spend on its development by all major bearing manufacturers, no product solution has come to market yet. This can be attributed to both the complexity in conditioning of the strain measurement as well as its nonlinearity with respect to the bearing loading. To address these issues, this paper proposes a novel approach based on modeling of the physical behavior of the bearing. An extended Kalman filter including a novel strain model is applied for signal conditioning, whereas an unscented Kalman filter including a semianalytical bearing model is proposed for reconstruction of the bearing load. An experimental study in both laboratory and field conditions shows that the proposed cascaded Kalman filtering approach leads to accurate estimates for all four considered bearings loads in various loading conditions. Besides an improvement on accuracy, the novel approach leads to a reduction in calibration effort.**

***Index Terms*—Bearing modeling, condition monitoring, load reconstruction, rolling bearing.**

I. Introduction

ROLLING bearings are essential components in a wide variety of products and machinery allowing for the rotational motion of shafts. As their failing is one of the most common reasons for machinery breakdown [1], bearing diagnosis and fault detection are active fields of research. This is reflected by the various condition monitoring approaches as vibration, acoustic emission, sound pressure, lubrication, and thermal analyses that have been developed and applied [2]–[6].

Condition monitoring focuses on the detection of incipient bearing failure or remaining useful life estimation by the detection of (local) bearing defects [7] in order to schedule upkeep or replacement. Excessive loading, bearing misalignment, or improper loading are root causes for a considerable part of bearing defect initiation and growth. Bearing load monitoring would enable for the detection of these improper conditions and thereby allows for monitoring of the cause of defect initiation.

As bearings furthermore often form important connectivity points, load measurement could also provide valuable information at the system level. Of particular interest is the development of wheel-end load estimation as this would allow for improved vehicle dynamics control and safety systems such as load-based-state estimation [8], antilock braking [9], and chassis control [10].

Hence, it could serve as a valuable addition to condition monitoring as well as for system analysis and control. Due to these reasons, all major bearing manufactures work on the development of the bearing upgrade to load-cell [11]–[16].

Load monitoring on a bearing level can be based on two different physical quantities. Either the outer ring *deformation* is measured by the use of strain gauges [12], [17], [18], ultrasonic sensors [19], or optical fibers [20], or the relative inner- to outer ring *displacement* is determined by Hall effect [13], [21], eddy-current [22], [23], or capacitive [24] sensors. After signal conditioning, the measured physical quantities are translated to the bearing loading by empirical methods such as least squares fitting [12], [17] or artificial neural networks [25].

However, due to effects such as strain lumping and thermal drift, current deformation-based signal conditioning approaches are inapplicable for double row roller bearings as, for instance, found at vehicle wheel-ends. In this paper, these difficulties are addressed and a novel conditioning approach to overcome these issues is proposed. The latter is the first of two main contributions of this paper, and encompasses a novel strain model and its implementation in an extended Kalman filter (EKF).

Besides the problem of conditioning itself, the nonlinear relation between the conditioned signal and bearing loading is challenging to be effectively captured by the use of empirical methods. The latter is reflected by the case specific and/or partial solutions found for the load reconstruction phase [9], [12]. Although piecewise linearization [12] and higher order fitting [17] may lead to decent load estimates, the robustness and applicability of such approach for industrialization is debatable as it inevitably leads to numerous parameters subject to calibration. In order to capture the nonlinear relationship and minimize the calibration effort, the second contribution of this paper is the introduction of a model-based load reconstruction phase. The latter considers the implementation of a semianalytical bearing model in an unscented Kalman filter (UKF).

Manuscript received May 31, 2018; revised September 3, 2018, October 1, 2018, and December 10, 2018; accepted January 9, 2019. Date of publication February 11, 2019; date of current version August 30, 2019. *(Corresponding author: Stijn Kerst.)*

The authors are with the Mechanical Engineering Department, Delft University of Technology, 2628 Delft, The Netherlands (e-mail: kerst@arrival.com; b.shyrokau@tudelft.nl; eholweg@vmi-group.com).

Color versions of one or more of the figures in this paper are available online at http://ieeexplore.ieee.org.

Digital Object Identifier 10.1109/TIE.2019.2897510

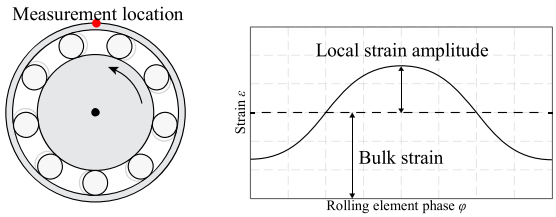

Fig. 1. Cyclic local strain behavior due to reallocation of rolling elements in a loaded running bearing.

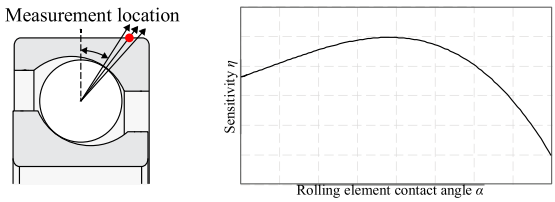

Fig. 2. Schematic representation of relationship between contact angle and measurement sensitivity η.

The paper is structured as follows. In Section II, bearing strain, conditioning, and its modeling are discussed. In Section III, the bearing load model is introduced. The implementation of the strain and load model in the Kalman filter-based algorithm is presented in Section IV. In Section V, the reference study is addressed. Section VI discusses the experimental setup after which the experimental results are presented and discussed in Section VII. Finally, Section VIII concludes this paper.

II. Bearing Strain

An important aspect in bearing strain conditioning is the differentiation between bulk and local deformation. In this section, both effects are elaborated and their signal conditioning methods are discussed. Finally, the novel *strain model* is proposed, which describes the relationship between the passing of loaded rolling elements and local outer ring strain.

A. Bulk and Local Deformation

The *bulk effect* or global deformation considers the average strain during a full passage of rolling elements as indicated in Fig. 1. It is directly affected by the applied bearing loading as well as by (pre-)stress due to thermal effects and boundary conditions. Its behavior is defined by bearing geometry, material properties, and boundary conditions.

The *local effects* are contributed to the rolling element contact loads and their continuous rearrangement,

Considering equally spaced rolling elements by a cage, the element rearrangement results in a periodic variation of load paths, stresses, and strains for any bearing load. Any location on the outer ring measuring the rolling element local contact deformation therefore will capture a cyclic strain for a running bearing. The location and properties of the strain measurement and local geometry determine the shape of the cyclic strain, of which an example is visualized in Fig. 1.

As depicted in Fig. 2, the sensitivity of the local strain to the local rolling element load is related to the rolling element load line or contact angle. Local geometry, material properties, and the axial location of the measurement point define the magnitude and shape of the contact angle sensitivity.

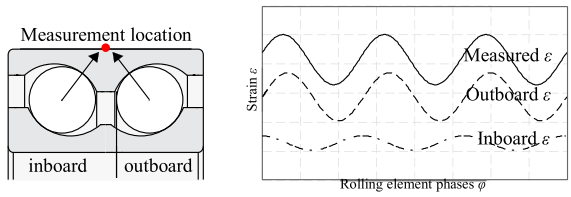

Fig. 3. Strain superposition of inboard and outboard local strain effects.

In the case of a double row bearing with little axial spacing between both raceways, any axially centered measurement location will capture a lumped measurement of both local inboard and outboard strain effects. Assuming linear elastic mechanical behavior, the superposition principle holds and hence the measured local strain is the sum of inboard and outboard local effects as depicted in Fig. 3.

B. Signal Conditioning

The bulk effect can be determined by specific strain gauge design [12] or notch/low-pass filtering [9]. As thermal effects on the bulk deformation however are significant and hard to address, it provides an inaccurate measure for reconstruction of the bearing loading.

By the use of a peak-to-peak detection algorithm [11], the local strain amplitude can be determined. Although effective when a single raceway is considered, this approach is inapplicable for any lumped strain measurement (see Fig. 3) as the amplitude of the super-positioned measurement is inconclusive; asynchronicity of the inboard and outboard rolling elements leads to varying phase differences, which on its turn affect the measured local strain amplitude. Current conditioning approaches furthermore are suboptimal with respect to noise suppression and signal bandwidth due to the basic signal processing involved.

To discriminate inboard and outboard local effects and for improved signal quality, a continuous model-based tracing by the use of Kalman filtering is proposed. In the following, the local strain model is proposed, which after implementation in the proposed algorithm is applied to determine the inboard and outboard rolling element loads from local strain measurements.

C. Local Strain Modeling Equations

Based on the behavior discussed in Section II-A, the following general strain approximation model is proposed for the local strain resulting from a single loaded rolling element:

$$\varepsilon_l(\psi) = Q(\psi)\, G(\varphi)\, \eta(\alpha) \tag{1}$$

where ε_l is the outer ring local strain at azimuth ψ, Q is the rolling element load at azimuth ψ, G is a normalized periodic transfer function dependent on the local rolling element phase φ, and η represents the measurement location sensitivity as a function of contact angle α.

The periodic transfer function captures the effect of the changing load paths on the outer ring local deformation. Assuming a constant rolling element load during the ball-passing period, the local strain variation can be fully addressed to the periodic

transfer function. The following representation is proposed:

$$G(\varphi) = \sum_{n=1}^{N_h} a_n \cos(\varphi n + \phi_n) \tag{2}$$

where a_n and ϕ_n represent the magnitude and relative phase shifts of each of the n harmonics and N_h defines the number of harmonics considered. The local rolling element phase φ is periodic with $-\pi \leq \varphi < \pi$ and equals 0 when an element is in line. Function normalization is achieved by setting the first harmonics' magnitude a_1 to unity and phase ϕ_1 to zero.

Due to the normalization of the periodic function, the element load to strain magnitude is solely reflected by the measurement location sensitivity. For the sensitivity, which is a function of contact angle α, the following polynomial description is proposed:

$$\eta(\alpha) = \sum_{n=0}^{N_p} c_n \alpha^n \tag{3}$$

where c_n are the polynomial coefficients and N_p is the order of the polynomial.

In case a double row bearing is considered, the right-hand side of (1) can be extended by a similar description for the second raceway according to the superposition principle.

III. Bearing Load Model

This section presents the *bearing load model,* which relates the previously described inboard and outboard rolling element loads to the bearing loading. As both real-time implementation and raceway deformation are considered important, this paper implements the semianalytical model as introduced in [26]. In the following, the bearing modeling equations are presented.

A. Modeling Equations

The rolling element normal force Q at any azimuth angle Ψ is described as a function of the local normal approach of both raceways

$$Q(\psi) = K_n \delta(\psi)^{3/2} \tag{4}$$

where δ is the raceway normal approach at azimuth ψ and K_n is the load-deflection factor. The inner ring position and orientation are defined by 5 degrees of freedom. The outer ring is modeled as flexible whilst its position is fixed. For any bearing azimuth angle ψ this results in the following description of normal approach δ and contact angle α

$$\delta(\psi) = \Big[(R_i + \delta_x \cos(\psi) + \delta_y \sin(\psi) - (R_o + u_r(\psi)))^2 + (Z_i + \delta_z + R_i\gamma_x \sin(\psi) + R_i\gamma_y \cos(\psi) - Z_o)^2\Big]^{1/2} - A \tag{5}$$

$$\alpha(\psi) = \tan^{-1}\left(\frac{(Z_i + \delta_z + R_{i0}\gamma_x \sin(\psi) + R_i\gamma_y \cos(\psi) - Z_o)}{R_i + \delta_x \cos(\psi) + \delta_y \sin(\psi) - (R_o + u_r(\psi))}\right) \tag{6}$$

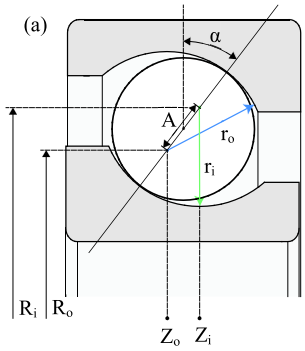

Fig. 4. Bearing section view showing bearing parameters.

where R_i, R_o, Z_i, Z_o, and A are bearing geometry parameters as indicated in Fig. 4, $\delta_x, \delta_y, \delta_z$ are the inner ring translations in x-, y-, and z-direction, γ_x and γ_y are the inner ring rotations over x- and y-axes. Finally, u_r is the radial static elastic outer raceway deformation. The latter is defined as follows:

$$u_r(\psi) = \mathbf{K}^{-1}\mathbf{Q} \tag{7}$$

where $\mathbf{K}^{-1}$ is the outer ring inverse stiffness matrix and $\mathbf{Q}$ the vector of all rolling element loads. The inverse stiffness or compliance matrix represents the nonlinear relationship between element loads and raceway deformation. In line with [26] the compliance matrix is approximated by

$$\mathbf{K}^{-1} = \varphi(\psi)\,\boldsymbol{\Theta}(\Psi) \tag{8}$$

where $\boldsymbol{\varphi}(\psi)$ is a column vector of normalized orthogonal deformation shapes and $\boldsymbol{\Theta}(\Psi)$ is a row vector of a Fourier-series-based compliance approximation. The latter is determined by the use of a finite-element study on the bearing outer ring structure. For a detailed description of the race deformation modeling, the reader is referred to [26].

The bearing forces and moments are calculated by summation of the rolling element load vector as follows:

$$\begin{aligned}
F_{Bx} &= \sum_{n=1}^{N_{\mathrm{re}}} Q(\psi_n)\cos(\alpha_n)\cos(\psi_n)\\
F_{By} &= \sum_{n=1}^{N_{\mathrm{re}}} Q(\psi_n)\cos(\alpha_n)\sin(\psi_n)\\
F_{Bz} &= \sum_{n=1}^{N_{\mathrm{re}}} Q(\psi_n)\sin(\alpha_n)\\
M_{Bx} &= \sum_{n=1}^{N_{\mathrm{re}}} R_m Q(\psi_n)\sin(\alpha_n)\sin(\psi_n)\\
M_{By} &= \sum_{n=1}^{N_{\mathrm{re}}} R_m Q(\psi_n)\sin(\alpha_n)\cos(\psi_n)
\end{aligned} \tag{9}$$

where n represents the rolling element index, N_{re} is the number of rolling elements and R_m is the bearing pitch radius which equals $(R_i + R_o)/2$.

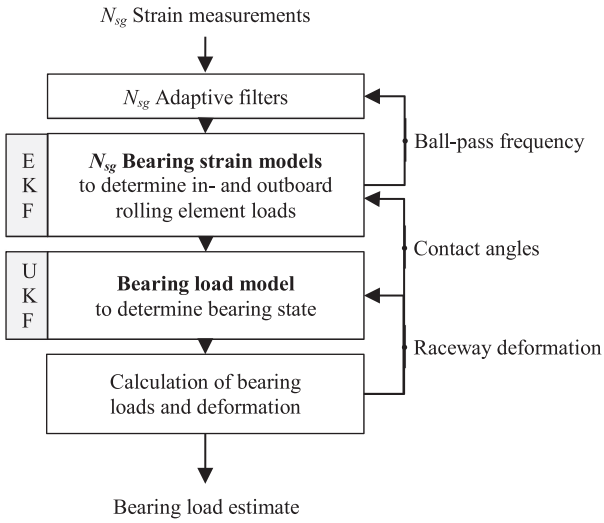

Fig. 5. Block diagram of the bearing load reconstruction algorithm.

IV. Novel Load Estimation Algorithm

Using the modeling equations presented in previous sections, a four-stage algorithm is proposed for the estimation of bearing loads based on strain measurement on the bearing outer ring. The algorithm, shown in the overview in Fig. 5, is characterized by two subsequent nonlinear Kalman filters. The first filter, an EKF, implements the strain model for translation of local strains to rolling element loads. The second UKF includes the bearing load model for translation of these element loads to the bearing state. The bearing state is then used for calculation of the bearing loading and to update the raceway deformation.

For computational efficiency, the first filter is of the EKF type, whereas an UKF is applied in the second stage due to the high nonlinearity of the model. Besides for simplified tuning, furthermore, a cascaded approach is chosen as two independent physical phenomena without cross covariance are described.

In the following, a generalized description of the algorithm is provided assuming a double row bearing equipped with N_{sg} strain gauges.

A. Adaptive Filtering

In this first stage of the algorithm, all N_{sg} strain measurements are filtered to extract the local strain effects from the raw measurements. Adequate separation of bulk and local effects is only possible when the ball-pass frequency exceeds the bandwidth of the external load. The latter is considered either static and known or dynamic and related to the rotational frequency of the bearing. The local strain is extracted by the use of a second-order Butterworth high-pass filter with cutoff frequency f_c according to

$$f_c = c_{\mathrm{bw}} \bar{f}_{\mathrm{bw}} \quad \text{if } \bar{f}_{\mathrm{bw}} = \text{cons.} \tag{10}$$

$$f_c = c_{\mathrm{bp}} f_{\mathrm{bp}} \quad \text{if } \bar{f}_{\mathrm{bw}} \neq \text{cons.} \tag{11}$$

where $\bar{f}_{\mathrm{bw}}$ is the upper frequency of the static bearing load bandwidth, f_{bp} is the ball-pass frequency estimate, and c_{bw} (>1) and c_{bp} (<1) are tuning constants providing separation between bulk deformation and ball-pass frequencies. The case-specific tuning constants should be chosen such that in operating conditions the high-pass filter provides respectively maximal and minimal attenuation of low- and high-frequency content so as to maximize the signal-to-noise ratio of the local strain.

Note that the separation of local strain from the raw measurement forms a fundamental requirement on the minimal bearing rotational speed.

Extended Kalman Filter Equations

Initialization

$$\hat{\mathbf{x}}_{n,0} = E\left[\mathbf{x}_n\right]$$

$$\mathbf{P}_{n,0} = E\left[(\mathbf{x}_n - \hat{\mathbf{x}}_{n,0})(\mathbf{x}_n - \hat{\mathbf{x}}_{n,0})^T\right]$$

1) *Time update*

$$\hat{\mathbf{x}}^-_{n,k} = \mathbf{F}\hat{\mathbf{x}}_{n,k-1}$$

$$\mathbf{P}^-_{n,k} = \mathbf{F}\mathbf{P}_{n,k-1}\mathbf{F}^T + \mathbf{Q}_{n,k}$$

2) *Measurement update*

$$\mathbf{K}_{n,k} = \mathbf{P}^-_{n,k}\mathbf{H}^T_{n,k}\left(\mathbf{H}_{n,k}\mathbf{P}^-_{n,k}\mathbf{H}^T_{n,k} + \mathbf{R}_{n,k}\right)^{-1}$$

$$\hat{\mathbf{x}}_{n,k} = \hat{\mathbf{x}}^-_{n,k} + \mathbf{K}_{n,k}\left(\mathbf{y}_{n,k} - f(\hat{\mathbf{x}}^-_{n,k}, \mathbf{u}_{n,k})\right)$$

$$\mathbf{P}_{n,k} = \mathbf{P}^-_{n,k} - \mathbf{K}_{n,k}\mathbf{H}_{n,k}\mathbf{P}^-_{n,k}$$

where $\mathbf{H}_{n,k} = \partial f(\hat{\mathbf{x}}^-_{n,k})/\partial\hat{\mathbf{x}}^-_{n,k}$, which is the linearization of the output equation at the current state estimate.

B. Strain Model-Based Extended Kalman Filter

The *strain model* is implemented in a parallel EKF approach to estimate local inboard and outboard rolling element loads, phases, and frequencies from the N_{sg} local strain measurements. For each local strain signal, a separate filter is set up according to the description as follows.

The EKF system equations are defined as follows:

$$\begin{aligned}\mathbf{x}_{n,k} &= \mathbf{F}\mathbf{x}_{n,k-1} + \mathbf{w}_n \\ \mathbf{y}_{n,k} &= f(\mathbf{x}_{n,k}, \mathbf{u}_{n,k}) + \mathbf{v}_n\end{aligned} \tag{12}$$

where $\mathbf{x}_n$ and $\mathbf{y}_n$ are respectively the state and measurement vector of the nth filter, $\mathbf{F}$ is the linear process model, f is the nonlinear measurement model, $\mathbf{u}_n$ is the external input vector, and $\mathbf{w}_n$ and $\mathbf{v}_n$ are the nth filter process and measurement noise matrixes, respectively, which are assumed as zero-mean Gaussian white noise with covariance $\boldsymbol{Q}_n$ and $\boldsymbol{R}_n$. The state, measurement, and external input vector are defined as follows:

$$\mathbf{x}_{n,k} = \left[\omega_{n,i,k} \quad \varphi_{n,i,k} \quad Q_{n,i,k} \quad \omega_{n,o,k} \quad \varphi_{n,o,k} \quad Q_{n,o,k}\right]^T \tag{13}$$

$$\mathbf{y}_{n,k} = \left[\varepsilon_{n,l,k} \quad \bar{\omega}_{i,k} \quad \bar{\omega}_{o,k}\right]^T \tag{14}$$

$$\mathbf{u}_{n,k} = \left[\alpha_{n,i,k} \quad \alpha_{n,o,k}\right]^T \tag{15}$$

where ω is the ball-pass frequency, $\varepsilon_{n,l}$ is the local strain determined by the adaptive filtering phase, $\bar{\omega}_i$ and $\bar{\omega}_o$ are pseudo measurements of the ball-pass frequency, and $\alpha_{n,i}$ and $\alpha_{n,o}$ are the rolling element contact angles obtained from the bearing load calculation stage. The i and o subscripts refer to inboard and outboard effects, respectively.

The ball-pass frequency pseudo measurements are added to avoid observability issues during low excitation of the respective raceways and equal the current most trusted estimated ball-pass frequency. The linear process model $\mathbf{F}$ is defined as the identity matrix with two off-diagonal terms on (2, 1) and (5, 4) equaling $1/t_s$, where t_s is the sampling period, to increment inboard and outboard phases with the current respective rotational frequency estimates.

C. Load Model-Based Unscented Kalman Filter

The *bearing load model* is implemented in an UKF to estimate the bearing state based on the estimated rolling element loads. The UKF system equations are defined as follows:

$$\begin{aligned}\mathbf{x}_{b,k} &= \mathbf{x}_{b,k-1} + \mathbf{w}_b \\ \mathbf{y}_{b,k} &= g(\mathbf{x}_{b,k}, \mathbf{u}_{b,k}) + \mathbf{v}_b\end{aligned} \tag{16}$$

where $\mathbf{x}_b$ is the state vector, $\mathbf{y}_b$ is the measurement vector, g is the nonlinear measurement model, $\mathbf{u}_b$ is the external input vector, and $\mathbf{w}_b$ and $\mathbf{v}_b$ are the process and measurement noise which are assumed to be zero-mean Gaussian white noise with covariance of, respectively, $\boldsymbol{Q}_b$ and $\boldsymbol{R}_b$. Note that no process model is described as it equals the identity matrix. The state, measurement, and external input vector are defined as follows:

$$\mathbf{x}_b = \begin{bmatrix}\delta_x & \delta_y & \delta_z & \gamma_x & \gamma_y\end{bmatrix}^T \tag{17}$$

$$\mathbf{y}_b = \begin{bmatrix}\delta_{i,1} & \delta_{o,1} & \cdots & \delta_{i,N_{\mathrm{sg}}} & \delta_{o,N_{\mathrm{sg}}}\end{bmatrix}^T \tag{18}$$

$$\mathbf{u}_b = \begin{bmatrix}u_r\left(\psi_1\right) & \cdots & u_r\left(\psi_{N_{\mathrm{sg}}}\right)\end{bmatrix}^T \tag{19}$$

where the measurement vector consists of the normal approaches calculated using the previously estimated rolling element loads by (4). This transformation is applied as this leads to a better convergence of the bearing model due to the nature of (4) that results in a discontinuity in the calculated element load. The raceway deformation is regarded as external input and is obtained from the subsequent bearing model calculation phase.

D. Calculation of Bearing Load and Deformation

Using the UKF state vector and (4)–(9), all rolling element loads, contact angles, and subsequent bearing loads can be calculated based on the current raceway deformation estimate. The calculated rolling element loads are then used for updating the deformation estimate by (7) and (8).

V. Reference Load Estimation Algorithm

The results of the novel estimation approach are assessed by a comparison study to a state-of-the-art bulk deformation—coefficient based load estimation algorithm by combining features of [12] and [17]. The algorithm, shown in the overview in Fig. 6, applies a second-order Butterworth low-pass filter with a cutoff frequency of 10 Hz to determine the bulk deformation. After offsetting the filtered measurements by the use of thermal offset vector $\boldsymbol{\zeta}$, the bearing loads are calculated

$$\mathbf{y}_r = \mathbf{x}_r\boldsymbol{\beta} + \mathbf{v}_r \tag{20}$$

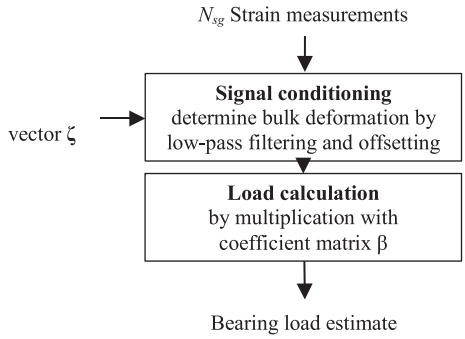

Fig. 6. Block diagram of the reference load estimation algorithm.

Unscented Kalman Filter equations

Initialization

$$\hat{\mathbf{x}}_{b,0} = E\left[\mathbf{x}_b\right]$$

$$\mathbf{P}_{b,0} = E\left[\left(\mathbf{x}_b - \hat{\mathbf{x}}_{b,0}\right)\left(\mathbf{x}_b - \hat{\mathbf{x}}_{b,0}\right)^T\right]$$

$$W_0^c = \lambda/\left(L+\lambda\right) + \left(1-\alpha^2+\beta\right)$$

$$W_i^c = 1/\left(2\left(L+\lambda\right)\right) \quad i = 1, \ldots, 2L$$

1) *Time update*

$$\hat{\mathbf{x}}_{b,k}^- = \hat{\mathbf{x}}_{b,k-1}$$

$$\mathbf{P}_{b,k}^- = \mathbf{P}_{b,k-1} + \mathbf{Q}_{b,k}$$

$$\mathbf{X}_{b,k}^- = \left[\hat{\mathbf{x}}_{b,k}^- \quad \hat{\mathbf{x}}_{b,k}^- + \gamma\sqrt{\mathbf{P}_{b,k}^-} \quad \hat{\mathbf{x}}_{b,k}^- - \gamma\sqrt{\mathbf{P}_{b,k}^-}\right]$$

$$\mathbf{Y}_{b,k}^- = g(\mathbf{X}_{b,k}^-, \mathbf{u}_{b,k})$$

$$\hat{\mathbf{y}}_{b,k}^- = g(\hat{\mathbf{x}}_{b,k}^-, \mathbf{u}_{b,k})$$

2) *Measurement update*

$$\mathbf{P}_{\hat{\mathbf{y}}_{b,k}\hat{\mathbf{y}}_{b,k}} = \sum_{i=0}^{2L} W_i^c \left(\mathbf{Y}_{b,k}^- - \hat{\mathbf{y}}_{b,k}^-\right)\left(\mathbf{Y}_{b,k}^- - \hat{\mathbf{y}}_{b,k}^-\right)^T + \mathbf{R}_{b,k}$$

$$\mathbf{P}_{\hat{\mathbf{x}}_{b,k}\hat{\mathbf{y}}_{b,k}} = \sum_{i=0}^{2L} W_i^c \left(\mathbf{X}_{b,k}^- - \hat{\mathbf{x}}_{b,k}^-\right)\left(\mathbf{Y}_{b,k}^- - \hat{\mathbf{y}}_{b,k}\right)^T$$

$$\mathbf{K}_{b,k} = \mathbf{P}_{\hat{\mathbf{x}}_{b,k}\hat{\mathbf{y}}_{b,k}}\mathbf{P}_{\hat{\mathbf{y}}_{b,k}\hat{\mathbf{y}}_{b,k}}^{-1}$$

$$\hat{\mathbf{x}}_{b,k} = \hat{\mathbf{x}}_{b,k}^- + \mathbf{K}_{b,k}\left(\mathbf{y}_{b,k} - \hat{\mathbf{y}}_{b,k}^-\right)$$

$$\mathbf{P}_{b,k} = \mathbf{P}_{b,k}^- - \mathbf{K}_{b,k}\mathbf{P}_{\hat{\mathbf{y}}_{b,k}\hat{\mathbf{y}}_{b,k}}\mathbf{K}_{b,k}^T$$

where α and β control the sigma point spread, L is the length of the state vector and λ is defined as $\lambda = \alpha^2 L - L$.

TABLE I
STRAIN GAUGE SPECIFICATIONS

Type	CEA-06-062UR-350	**Pattern Type**	Rectangular Rosette
Strain range	±3%	**Active length**	1.57 mm
Resistance	350 Ohms	**Active width**	1.57 mm
Gauge factor	2.150 ± 0.5%	**Operating temp.**	-75~175ºC

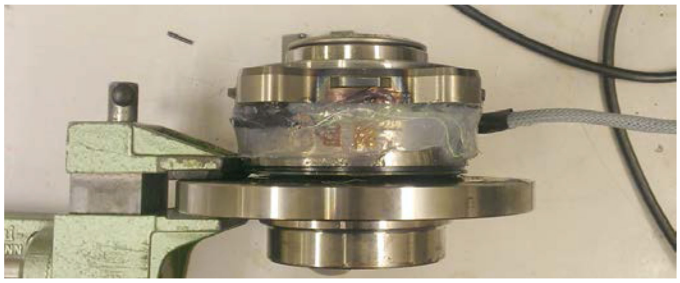

Fig. 7. Instrumented bearing before mounting on the test setup.

where $\mathbf{y}_r$ is the vector of bearing load estimates, $\mathbf{x}_r$ is the deformation vector, $\boldsymbol{\beta}$ is the coefficient matrix, and $\mathbf{v}_r$ is the noise term. The deformation vector $\mathbf{x}_r$ is defined as follows:

$$\mathbf{x}_r = \begin{bmatrix} \varepsilon_{b,1} & \cdots & \varepsilon_{b,N_{\mathrm{sg}}} & \varepsilon_{b,1}^2 & \cdots & \varepsilon_{b,N_{\mathrm{sg}}}^2 \end{bmatrix} \tag{21}$$

where ε_b is the outer ring bulk deformation offsetted by the offset vector $\boldsymbol{\zeta}$. The latter is applied to compensate for thermal drift of the bulk deformation.

VI. EXPERIMENTAL SETUP

A. Bearing Instrumentation

The outer ring of a BMW 5-series front wheel-end bearing is instrumented with four $(N_{\mathrm{sg}} = 4)$ general-purpose strain gauges at a 90° interval over the bearing circumference. The gauges are placed in line with the principal axis of the bearing as the paper aims to estimate radial forces and moments over these two axis. Due to the tight axial raceway spacing, each strain gauge considers a lumped inboard and outboard strain measurement. The strain gauges, specified in Table I, are applied in a Wheatstone bridge setup and amplified using a Peekel 9236 type conditioner. A layer of silicone is applied to protect the strain gauges and wiring from the harsh wheel-end environment. Fig. 7 shows the instrumented bearing before mounting.

B. Laboratory and Field Test Setup

A dedicated bearing test rig is used for testing in laboratory conditions. The test rig, shown in Fig. 8, allows for dynamic loading of all five relevant degrees of freedom by the use of force controlled hydraulic actuators while rotating the bearing with an electric motor. Besides the instrumented bearing, the setup includes the steering knuckle to more closely resemble vehicle implementation. Data acquisition is performed by the use of a Yokogawa DL750P mixed signal oscilloscope at a sampling rate of 2 kHz.

The field tests are performed on a BMW 5-series E60 type production vehicle at an old airstrip. The test vehicle, shown in Fig. 9, is equipped with a vehicle load sensor wheel force transducer [27] that serves as reference load measurement. Data acquisition is performed by the use of a dSpace Autobox at a sampling rate of 500 Hz.

The algorithm is implemented in MATLAB/Simulink and applied offline on the data acquired during experiments on both test setups.

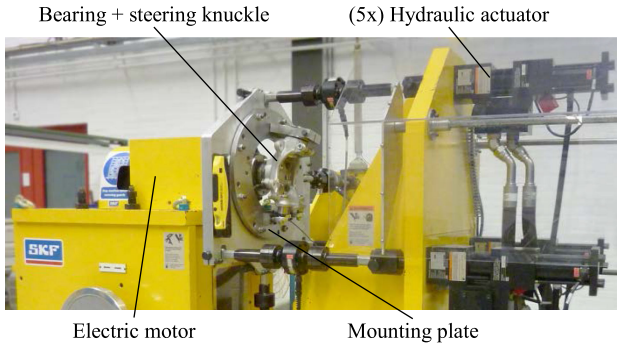

Fig. 8. Bearing test system located at our industrial partner.

Fig. 9. Instrumented test vehicle including load sign convention.

TABLE II
TOTAL COMBINED EXCITATION RANGE OF CALIBRATION AND VALIDATION EXPERIMENTS

Load		**Min**	**Max**
Longitudinal force	F_x	-5.5 kN	0.5 kN
Vertical force	F_z	1.5 kN	10.0 kN
Over-turning moment	M_x	-0.7 kNm	2.1 kNm
Self-aligning moment	M_z	-0.4 kNm	0.2 kNm

C. Experimental Study

The presented results consider two load cases on the bearing test system and one on the test vehicle. All tested loading conditions consider realistic wheel-end bearing loads.

For each load case, a qualitative and quantitative analysis based on time domain results and root-mean-square error (RMSE) is provided. The RMSE results are provided in both absolute and relative terms, where the latter is related to the full experimental excitation range as indicated in Table II.

The load cases are evaluated on the estimation accuracy of longitudinal force F_x, vertical force F_z, tilting moment M_x, and

self-aligning moment M_z according to the sign convention as indicated in Fig. 9. Lateral force F_y is omitted as it was found that the setup with only four strain gauges provides insufficient information for accurate estimation.

The laboratory and field data results are filtered using a second-order Butterworth low-pass filter with cutoff frequencies of respectively 4 and 1 Hz.

D. Parameter Definition and Calibration

As the *bearing load model* is a well-established and validated modeling part, its parameters are defined *a priori* so as to minimize the calibration effort. By the use of technical drawings, the geometrical parameters are defined whilst the bearing compliance is determined by a finite-element study in line with [26].

Quantification of the introduced *strain model* parameters is achieved by the use of a calibration routine. The order of the periodic transfer function and sensitivity polynomial are set to $N_h = 2$ and $N_p = 3$, respectively. As the bearing is plane symmetric, the front and rear strain model parameters are considered to be equal, resulting in a total of 18 parameters for calibration.

The parameters are calibrated by a nonlinear least squares minimization procedure of the radial forces and accompanying moments based on a total of 166 s of test rig experiments containing various road realistic load cases. In line with common practice, none of the presented load cases in the results section are in the calibration set.

E. Algorithm Initialization and Tuning

For initialization of the algorithm, only the initial rotational frequency is required as prior knowledge. In the experimental setup, this is obtained from the wheel speed encoders; however, this could also be estimated based on the raw strain signals using a frequency estimator.

As common in the application of Kalman filtering, the process and measurement noise covariance matrixes are tuned for improved convergence and robustness of the nonlinear filters. As the strain gauge excitation varies significantly, a rule-based tuning is applied based on internal filter states.

F. Reference Study Setup

The 32 coefficients in matrix $\boldsymbol{\beta}$ are determined by a multivariate linear least squares regression analysis using the same 166 s of test rig experiments as used for the calibration of the proposed algorithm. The thermal offset vector $\boldsymbol{\zeta}$ for compensation of thermal drift is recalibrated on a regular basis during unloaded conditions (test rig, every 5 min) and lifting of the wheel (test vehicle, every half an hour) to avoid large estimation errors.

VII. Experimental Results and Discussion

In this section, the three experiments are presented, followed by an overall discussion in Section VII-D.

A. Test Rig: Cornering and Braking Combined Loading

This first load case considers the bearing loads during cornering and braking to analyze the estimation results for combined loading. The experiment is performed on the bearing test rig at a constant rotational speed of 1000 r/min, resembling a driving speed of approximately 120 km/h. The time domain results and quantitative evaluation are presented in Fig. 10 and Table III, respectively.

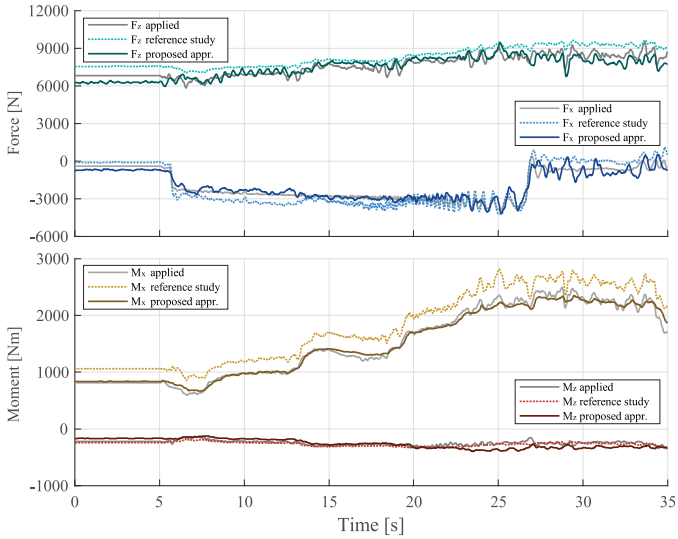

Fig. 10. Time domain results of load case 1 performed on the bearing test rig.

TABLE III
RMSE of Load Case 1

Load		Reference study		Proposed approach	
Longitudinal force	F_x	529 N	8.8 %	375 N	6.3 %
Vertical force	F_z	725 N	8.5 %	439 N	5.2 %
Tilting moment	M_x	290 Nm	10.4 %	64 Nm	2.3 %
Self-aligning moment	M_z	30 Nm	4.9 %	64 Nm	10.7 %

The time domain results show good quasi-static tracking of all loads determined by the proposed approach, whereas significant errors on both forces and tilting moment M_x are noted for the reference study. The results furthermore show that the precision of the longitudinal force F_x by the proposed approach decreases as overall bearing loading increases.

The RMSE results confirm that the proposed approach outperforms the reference study on all loads except for the low excited self-aligning moment M_z.

B. Test Rig: Slalom Maneuver

The second load case regards the loading during a slalom maneuver to analyze the estimation quality for large internal load variations. The test is performed at a constant rotational speed of 1000 r/min. Fig. 11 shows the load case results over time for vertical force F_z and tilting moment M_x as well as the indication of the time domain used for the quantitative results presented in Table IV.

From the time domain results, different regions in estimation quality can be observed for the proposed approach; during the application of tilting moment M_x, a good tracking is observed whilst large errors are encountered in the switching periods in-between. The erroneous periods, which are related to difficulties in the EKF strain filters, are addressed in the discussion section.

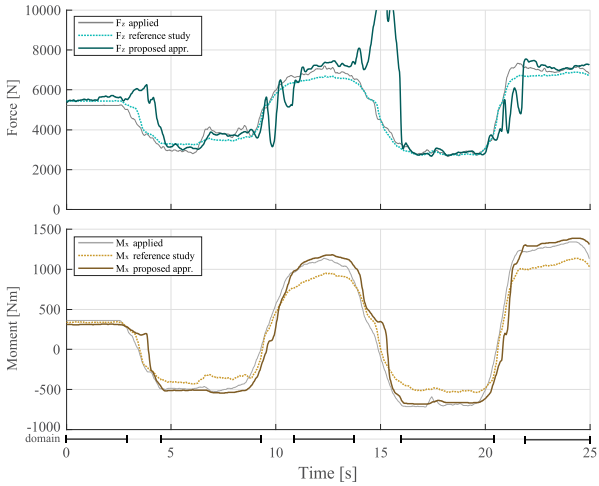

Fig. 11. Time domain results of load case 2 performed on the bearing test rig including the domain indication for the quantitative results of Table IV.

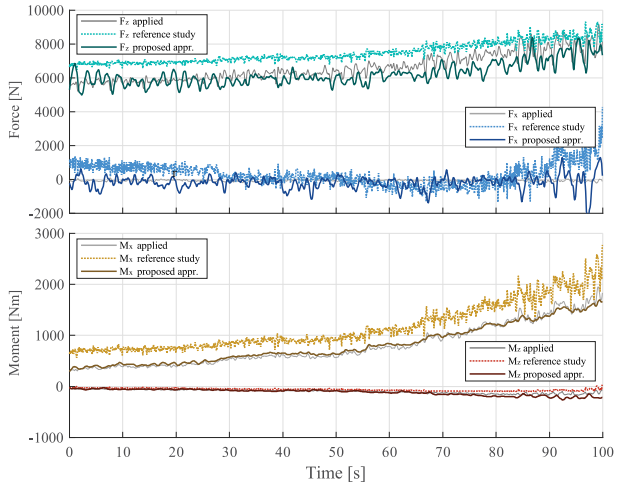

Fig. 12. Time domain results of load case 3 performed on the test vehicle.

TABLE IV
RMSE OF INDICATED TIME DOMAIN LOAD CASE 2

Load		Reference study		Proposed approach	
Longitudinal force	F_x	197 N	3.3 %	473 N	7.9 %
Vertical force	F_z	269 N	3.2 %	275 N	3.2 %
Tilting moment	M_x	155 Nm	5.5 %	68 Nm	2.4 %
Self-aligning moment	M_z	42 Nm	7.0 %	22 Nm	3.6 %

TABLE V
RMSE OF LOAD CASE 3

Load		Reference study		Proposed approach	
Longitudinal force	F_x	711 N	11.9 %	416 N	6.9 %
Vertical force	F_z	897 N	10.6 %	624 N	7.3 %
Tilting moment	M_x	356 Nm	12.7 %	77 Nm	2.8 %
Self-aligning moment	M_z	41 Nm	6.8 %	34 Nm	5.7 %

It is noted that the bulk deformation-based reference study is not affected during the inboard/outboard switching periods. However, an underestimation of tilting moment M_x is encountered in cornering conditions.

The quantitative results, focused only on the stable estimation domain, show similar performance of the proposed algorithm to load case 1. The reference study performs considerably better with respect to load case 1.

C. Test Vehicle: Cornering

This last load case considers a cornering maneuver on the test vehicle. The test is performed at a slowly increasing driving speed from 35 to 60 km/h whilst a constant cornering radius of approximately 50 m is maintained. Time and quantitative results of this 100 s long experiment are presented in Fig. 12 and Table V, respectively.

Time domain results show good quasi-static load estimates by the proposed approach, although a slight underestimation of the vertical force F_z is observed. The reference study on the other hand shows considerable errors for all load estimates except self-aligning moment M_z. In line with load case 1, precision of the longitudinal force estimate F_x decreases as overall bearing loading increases.

The quantitative results confirm these observations as errors of the proposed approach are in line with load case 1 and 2, whilst a considerable increase in rms errors of longitudinal force F_x, vertical force F_z, and tilting moment M_x for the reference study is noted.

D. Discussion

The *proposed approach* leads an accurate estimation of all four considered loads in both laboratory as well as field conditions.

Only during switching of moment direction, erroneous load estimates are noted. These errors originate from the conditioning phase of the algorithm as the EKF has difficulties in discriminating the super-positioned strains during the inboard/outboard rolling element load transfer. This discrimination is made difficult as states change quickly whilst the amount of information is limited due to the low bearing loading and consequent deformation. However, the Kalman filter recovers after switching of moment direction showing the overall robustness of the approach.

The decrease of precision of the low-excited longitudinal force estimate F_x during load case 1 and 3 is attributed to cross coupling as the rolling element load distribution is dependent on all five bearing loads whilst strain gauge locations are fixed. Due to the former, any individual load can be reflected by various rolling element load distributions. The latter consequently results in a varying sensitivity and precision depending on this load distribution.

The offset in vertical force estimate F_z during the field test is attributed to minor differences in boundary conditions with respect to the laboratory setup.

The *reference study* shows large errors in the estimation of longitudinal force F_x, vertical force F_z, and the overturning moment M_x. The origin of these errors is twofold. The constant biases on vertical force F_z and tilting moment M_x during load case 1 and 3 are attributed to thermal effects. The varying

estimation errors, as the underestimation of tilting moment M_x in load case 2 and varying under- and overestimation of longitudinal force F_x during load case 1 and 3, on the other hand, find their origin in the coefficient-based load calculation.

Overall, it is observed that for both methods, moments are more accurately estimated than forces. This is a consequence of the relatively larger bulk and local deformation resulting from moment loading.

It can be noted that, even with regular recalibration of the thermal offset vector $\boldsymbol{\zeta}$, thermal drift is the weak point of the bulk deformation-based conditioning of the reference study. Due to conditioning focused on local strain, the proposed algorithm is invariant to these thermal effects resulting in better estimates and a good repeatability.

Focusing on the load reconstruction phase, omitting thermal effects, one could conclude that the model-based load reconstruction leads to only a minor increase in estimation accuracy. However, the main advantages of the application of a model-based approach with respect to a data-driven method are in calibration and its robustness. Due to modeling and usage of bearing physical parameters, the number of parameters subject to calibration is reduced. As principal relationships are furthermore defined *a priori,* the risk of overfitting decreases and calibration effort is reduced.

VIII. Conclusion

This paper presented a novel model-based strain conditioning and load calculation phase for the purpose of bearing load estimation. A cascaded extended and unscented Kalman filtering approach, including a novel strain model and semianalytical bearing model, was proposed. An experimental study covering both laboratory and field tests showed that the novel approach led to accurate load estimates in various conditions and outperforms the reference study. Of particular interest are the relatively low rms errors of 6.9% and 7.3% for longitudinal force F_x and vertical force F_z and 2.8% and 5.7% for tilting moment M_x and self-aligning moment M_z obtained during the field tests whilst calibration was conducted in laboratory conditions only. The results showed that the proposed local strain-based conditioning approach is invariant to thermal effects and leads to a good repeatability. The model-based load reconstruction phase of the algorithm furthermore improves accuracy whilst the risk of overfitting decreases and calibration effort is reduced.

Future work should focus on achieving an accurate and robust load estimate over the full (case specific) excitation range for any considered bearing. Of particular interest is the effect of the amount and location of strain gauges with respect to the estimation accuracy. Next to that a substantial improvement could be achieved by bearing shape optimization specifically for load estimation.

References

[1] T. Williams, X. Ribadeneira, S. Billington, and T. Kurfess, "Rolling element bearing diagnostics in run-to-failure lifetime testing," *Mech. Syst. Signal Process.*, vol. 15, pp. 979–993, 2001.

[2] N. Tandon and A. Choudhury, "A review of vibration and acoustic measurement methods for the detection of defects in rolling element bearings," *Tribol. Int.*, vol. 32, pp. 469–480, 1999.

[3] I. El-Thalji and E. Jantunen, "A summary of fault modelling and predictive health monitoring of rolling element bearings," *Mech. Syst. Signal Process.*, vol. 60–61, pp. 252–272, 2015.

[4] H. de Azevedo, A. Araújo, and N. Bouchonneau, "A review of wind turbine bearing condition monitoring: State of the art and challenges," *Renewable Sustain. Energy Rev.*, vol. 56, pp. 368–379, 2016.

[5] J. Lee, F. Wu, W. Zhao, M. Ghaffari, L. Liao, and D. Siegel, "Prognostics and health management design for rotary machinery systems—Reviews, methodology and applications," *Mech. Syst. Signal Process.*, vol. 42, pp. 314–334, 2014.

[6] J. Sun, C. Yan, and J. Wen, "Intelligent bearing fault diagnosis method combining compressed data acquisition and deep learning," *IEEE Trans. Instrum. Meas.*, vol. 67, no. 1, pp. 185–195, Jan. 2018.

[7] T. Liu and J. Mengel, "Intelligent monitoring of ball bearing conditions," *Mech. Syst. Signal Process.*, vol. 6, pp. 419–431, 1992.

[8] K. Nam, S. Oh, H. Fujimoto, and Y. Hori, "Estimation of sideslip and roll angles of electric vehicles using lateral tire force sensors through RLS and Kalman filter approaches," *IEEE Trans. Ind. Electron.*, vol. 60, no. 3, pp. 988–1000, Mar. 2013.

[9] S. Kerst, B. Shyrokau, and E. Holweg, "Antilock braking control based on bearing load sensing," in *Proc. EuroBrake*, Dresden, Germany, 2015, pp. 4–10.

[10] M. Gerard, "Global chassis control and braking control using tyre forces measurement," *Ph.D. thesis*, Delft Univ. Technol., Delft, The Netherlands, 2011.

[11] H. Mol, "Method and sensor arrangement for load measurement on rolling element bearing based on model deformation," U.S. Patent 7389701, 2008.

[12] K. Nishikawa, "Hub bearing with integrated multiaxis load sensor," NTN, Osaka, Japan, NTN Tech. Rev. no. 79, 2011.

[13] K. Ono, T. Takizawa, and M. Aoki, "Preload measuring device for double row rolling bearing unit," U.S. Patent 8864382, 2014.

[14] H. van der Knokke, R. Wunderlich, K. Hauser, and R. Hollweck, "Force-sensing bearing," U.S. Patent 7316168, 2008.

[15] M. Kraus and M. Bäuml, "Continuous wheel force measurement for passenger vehicles and commercial vehicles," in *Proc. 6th Int. Munich Chassis Symp.*, Munich, Germany, 2015, pp. 717–718.

[16] M. Baeuml *et al.*, "The chassis of the future," in *Proc. 10th Schaeffler Semin.*, 2014, pp. 392–411.

[17] H. A. Mol and G. C. van Nijen, "Method and sensor arrangement for load measurement on rolling element bearing," U.S. Patent No. 7.444.888, 2008.

[18] S. Kerst, B. Shyrokau, and E. Holweg, "Wheel force measurement for vehicle dynamics control using an intelligent bearing," in *Proc. 13th Int. Symp. Adv. Veh. Control*, 2016, pp. 547–552.

[19] W. Chen, R. Mills, and R. Dwyer-Joyce, "Direct load monitoring of rolling bearing contacts using ultrasonic time of flight," *Proc. Roy. Soc. A*, vol. 471, 2015, Art. no. 20150103.

[20] A. Reedman and H. Yang, "Bearing monitoring using a fibre bragg grating," U.S. Patent 8790013, 2014.

[21] K. Nam, "Application of novel lateral tire force sensors to vehicle parameter estimation of electric vehicles," *Sensors*, vol. 15, pp. 28385–28401, 2015.

[22] H. A. Mol, S. Van Ballegooij, and J. M. Storken, "Load determining system for a rolling element bearing," U.S. Patent 15/533, 545, 2016.

[23] K. Ayandokun, P. Orton, N. Sherkat, and P. Thomas, "Smart bearings: Developing a new technique for the condition monitoring of rotating machinery," in *Proc. IEEE Int. Conf. Intell. Eng. Syst.*, 1997, pp. 505–510.

[24] L. Rasolofondraibe, B. Pottier, P. Marconnet, and X. Chiementin, "Capacitive sensor device for measuring loads on bearings," *IEEE Sens. J.*, vol. 12, no. 6, pp. 2186–2191, Jun. 2012.

[25] H. A. Mol and G. C. van Nijen, "Method and sensor arrangement for load measurement on rolling element bearing," U.S. Patent No. 7.444.888, 2008.

[26] S. Kerst, B. Shyrokau, and E. Holweg, "A semianalytical bearing model considering outer race flexibility for model based bearing load monitoring," *Mech. Syst. Signal Process.*, vol. 104, pp. 384–397, 2018.

[27] A. Rupp, V. Grubisic, and J. Neugebauer, "Development of a multi-component wheel force transducer-a tool to support vehicle design and validation," SAE Tech. Paper 930258, 1993.

Stijn Kerst was born in Raamsdonk, The Netherlands, in 1986. He received the B.Sc. degree in industrial design engineering in 2009 and the M.Sc. degree in mechanical engineering in 2012 from the Delft University of Technology, Delft, The Netherlands, where he is currently working toward the Ph.D. degree in mechanical engineering.

He is working on the valorization of his research in industry; previously at SKF and currently with Arrival in London.

Barys Shyrokau was born in Barysaw, Belarus, in 1981. He received the Dipl.Eng. degree (cum laude) in mechanical engineering from Belarusian National Technical University, Minsk, Belarus, in 2004, and the joint Ph.D. degree in control engineering from Nanyang Technological University, Singapore, and Technical University Munich, Munich, Germany, in 2015.

He is an Assistant Professor in the Section of Intelligent Vehicles, Department of Cognitive Robotics, Delft University of Technology, Delft, The Netherlands. His research interests are related to vehicle dynamics and control, motion comfort and driving simulator technology.

Dr. Shyrokau was the recipient of scholarships and awards from the International Federation of Automotive Engineering Societies, German Academic Exchange Service, Singapore International Graduate Award, and International Society for Terrain-Vehicle Systems.

Edward Holweg was born in Maassluis, The Netherlands, in 1967. He received the M.Sc. and Ph.D. degrees in electrical engineering from the Delft University of Technology, Delft, The Netherlands, in 1990 and 1996, respectively.

He is currently working as a COO with the VMI Group, based in the Netherlands. From 2008–2017 he worked as a part-time Full Professor with the Faculty of 3ME (Mechanical, Maritime, and Materials Engineering), at the Delft University of Technology, in the area of Intelligent Automotive Systems. His research interests are related to vehicle dynamics and control, motion comfort and driving simulator technology.